WATER RESOURCES RESEARCH, VOL. 33, NO. 12, PAGES 2849–2863, DECEMBER 1997

# Stochastic forcing of sediment supply to channel networks from landsliding and debris flow

Lee Benda
Earth Systems Institute, Seattle, Washington

Thomas Dunne
School of Environmental Science and Management, University of California, Santa Barbara

**Abstract.** Sediment influx to channel networks is stochastically driven by rainstorms and other perturbations, which are discrete in time and space and which occur on a landscape with its own spatial variability in topography, colluvium properties, and state of recovery from previous disturbances. The resulting stochastic field of sediment supply interacts with the topology of the channel network and with transport processes to generate spatial and temporal patterns of flux and storage that characterize the sedimentation regime of a drainage basin. The regime varies systematically with basin area. We describe how the stochastic sediment supply is generated by climatic, topographic, geotechnical, and biotic controls that vary between regions. The general principle is illustrated through application to a landscape where sediment is supplied by mass wasting, and the forcing variables are deterministic thickening of colluvium, random sequences of root-destroying wildfires, and random sequences of rainstorms that trigger failure in a population of landslide source areas with spatial variance in topography and colluvium strength. Landslides stop in channels or convert to scouring debris flows, depending on the nature of the low-order channel network. Sediment accumulates within these channels for centuries before being transferred downstream by debris flows. Time series of sediment supply, transport, and storage vary with basin scale for any combination of climatic, topographic, and geotechnical controls. In a companion paper [*Benda and Dunne*, this issue] we use simulations of timing, volumes, and locations of mass wasting to study the interaction between a stochastically forced sediment supply and systematic changes of storage and flux through channel networks.

## 1. Introduction

Sediment influx to channel networks is inherently stochastic because it is driven by rainstorms and other perturbations that are discrete in time and space. The rainstorm climate of a drainage basin can be expressed as probability distributions of intensity, duration, interarrival time, and spatial dimension. Other stochastic processes that trigger hillslope erosion include earthquakes, windstorms, and fires of varying intensity and size that reduce vegetation cover, infiltration capacity, and root reinforcement. These stochastic processes, with their characteristic probability distributions, occur on landscapes over which there is considerable spatial variability in topography and soil properties, which may also vary through time, recording the history of earlier erosive events. Thus, sediment influx to channel networks occurs as a complex series of pulses, circumscribed in space and time, but with spatial and temporal characteristics (both immediately after a perturbation and as reflected over long periods in terms of frequency distributions) that can be quantitatively related to the stochastic factors listed above.

Here, we outline a framework for quantitative analysis of this general principle in a particular landscape in the central Oregon Coast Range (OCR, Figure 1) where sediment is introduced to channel networks mainly by landsliding and debris flows. Our analysis extends from landslide sources down first- and second-order channels, where the sediment budget is dominated by debris flows. In a companion paper [*Benda and Dunne*, this issue], we analyze some consequences of the interaction between a sediment supply that is stochastic in space and time and the fluvial sediment routing to be expected in a higher-order, dendritic channel network. Thus we deduce how the statistical properties of sediment supply and sediment storage in valley floors should vary systematically throughout channel networks in patterns that reflect various climatic, topographic, and lithologic controls. Later papers will illustrate the sensitivity of the results to a wider range of conditions.

Landslides and debris flows dominate the sediment budgets of many mountain drainage basins [*Dietrich and Dunne*, 1978; *Swanson et al*., 1982; *Pearce and Watson*, 1986; *Benda and Dunne*, 1987; *Ohmori and Hirano*, 1988]. Their deposits locally alter the morphology of streams, and this direct linkage between hillslopes and channels has been studied in many river basins [*Hack and Goodlett*, 1960; *Swanson and Lienkaemper*, 1978; *Ouchi*, 1987; *Benda*, 1990; *Perkins*, 1989]. Mass wasting also increases sediment supply, transport, and storage in the channel network, affecting water quality and the morphology of channels and valley floors. Transient downstream effects on channel and valley-floor morphology resulting from landslide-induced sediment supply include aggradation and subsequent incision [*Griffiths*, 1979; *Pickup et al*., 1983; *Lisle*, 1982; *Roberts*



Paper number 97WR02388.
0043-1397/97/97WR-02388$09.00

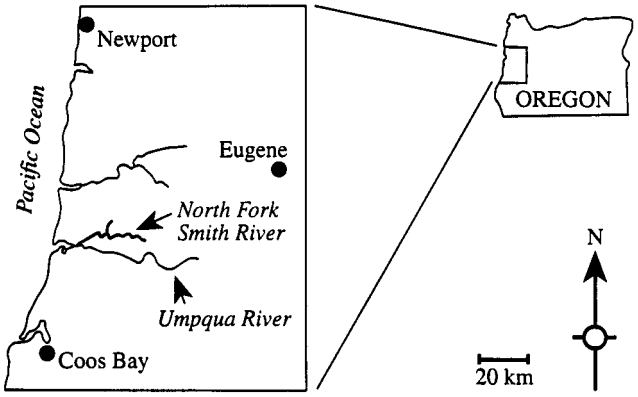


**Figure 1.** Location map showing western Oregon and the location of the North Fork Smith River where the simulation model was applied.

*and Church*, 1986], channel widening followed by narrowing [*Beschta*, 1984], fining of the substrate followed by coarsening [*Coates and Collins*, 1984; *Roberts and Church*, 1986], transformation of single channels to braided channels [*Roberts and Church*, 1986], decrease and then increase in the area and depth of pools [*Madej and Ozaki*, 1996], construction of terraces [*Hack and Goodlett*, 1960; *Roberts and Church*, 1986; *Nakamura*, 1986], and death of riparian forests [*Madej and Ozaki*, 1996].

Durations of changes in sediment supply from mass wasting range from years to decades [*Beschta*, 1984; *Pearce and Watson*, 1986], and lengths of affected channels extend up to tens of kilometers [*Griffiths*, 1979; *Beschta*, 1984; *Madej and Ozaki*, 1996]. Although many of the above-mentioned studies refer to mass wasting associated with land use, the effects listed above should also apply to naturally occurring mass wasting, which is also circumscribed in both space and time, although the frequency, magnitude, and spatial distribution of the morphological changes should be different.

Despite the widespread importance of mass wasting in mountain drainage basins, we know of no analysis of how the frequency and magnitude of sediment flux into and along channel networks are governed by climate- and landscape-specific controls on erosion processes, network structure, and spatial scale of the basin. Here and in a companion paper [*Benda and Dunne*, this issue] we propose a conceptual and simulation model of these interactions to examine the frequency and magnitude of sediment transport and storage in a network of first- through sixth-order channels. The analysis requires predicting the spatial and temporal behavior of the long-term (millennial) basin sediment budget (i.e., the frequency, magnitude, spatial distribution, and texture of sediment transported and stored by a number of interacting processes). This paper analyzes the factors that account for the frequency, magnitude, and spatial location of landsliding and debris flows. In order to obtain realistic values for critical variables, we have applied the simulation model to the 215 $km^2$ watershed of the North Fork Smith River (Figure 1) over a 3000-year period of the later Holocene.

Analysis of long-term sediment influx to channel networks introduces the complexities of large aggregates of hillslopes and long sequences of erosion events. To tackle the problem of increasing complexity, an upward approach [*Roth et al*., 1989, p. 320] is taken, which combines, by means of mathematical synthesis and computer simulation, empirical knowledge and theoretical reasoning available at smaller scales to produce new understanding at larger scales. This approach requires some degree of simplification in description and analysis of small-scale hillslope and channel processes and the use of estimated probability distributions to overcome limitations of data, computing resources, and knowledge of weather and fire sequences. Hence our objective is not numerical precision about future states at individual sites but rather to produce new, testable hypotheses on the relationship between the space-time structure of erosion and large-scale interactions of climate and topography. We use the central OCR as an example.

## 2. Landslide and Debris Flow Erosion in the OCR

The central OCR (Figure 1) is formed within massive beds of mechanically weak, marine sedimentary rocks [*Baldwin*, 1974]. Hillslopes have relief of up to several hundred meters. Colluvium, 0.1–0.5 m deep, mantles the planar portions of the 30°–40° hillslopes and migrates downhill into stream channels or into convergent areas of hillslopes called bedrock hollows or zero-order basins. In these hollows colluvium, stabilized by tree roots, accumulates over millennia to depths in excess of 2 m until root strength is no longer capable of stabilizing it when the pore pressure within it is elevated by large rainstorms. Wedges of colluvium are then evacuated as shallow landslides, the average frequency of which is controlled by the rate of colluvium production [*Dietrich and Dunne*, 1978]. The model of a self-driven cycle of hollow filling and evacuation has also been adopted in other mass wasting landscapes [*Hack and Goodlett*, 1960; *Tsukamoto and Minematsu*, 1987; *Crozier et al*., 1990]. Most shallow landslides in the OCR evolve into debris flows and scour other sediment that has accumulated in first- and second-order channels, depositing it at tributary junctions or in high-order reaches (Figure 2) [*Benda and Dunne*, 1987]. Because first- and second-order channels comprise approximately 90% of all channel length in the central OCR, debris flows in them are important to the sedimentation regime of higher-order channels.

Plant roots play a critical role in stabilizing colluvium against failure on mountain slopes, and thus the accumulation of sediment in hollows can be interrupted by landsliding when intense forest fires kill tree roots and are followed by large rainstorms before new root networks become established (Figure 3). The erosion resets the soil depth, beginning a new epicycle of thickening [*Dietrich and Dunne*, 1978]. Climate change that replaces or thins a forest cover or that increases the frequency of intense fires can also trigger episodes of landsliding [*Reneau and Dietrich*, 1990]. Thus considerable spatial and temporal variability in sediment production is reflected in the instrumental and alluvial records, and in the vulnerability of slopes to future erosion.

In an investigation of bedrock hollows in the OCR, *Reneau and Dietrich* [1991] interpreted the similarity between average, long-term (6000–15,000 years) hollow denudation rates ($n$ = 9) and modern (1960–1980) drainage basin sediment yields ($n$ = 9) to indicate approximate landscape equilibrium. Yet the denudation rates varied by a factor of 6, and the modern sediment yields by a factor of 3.5, indicating considerable spatial and temporal variability of erosion around this average condition. In addition, *Reneau and Dietrich* [1990] interpreted an apparent clustering of basal radiocarbon dates (4000–7500

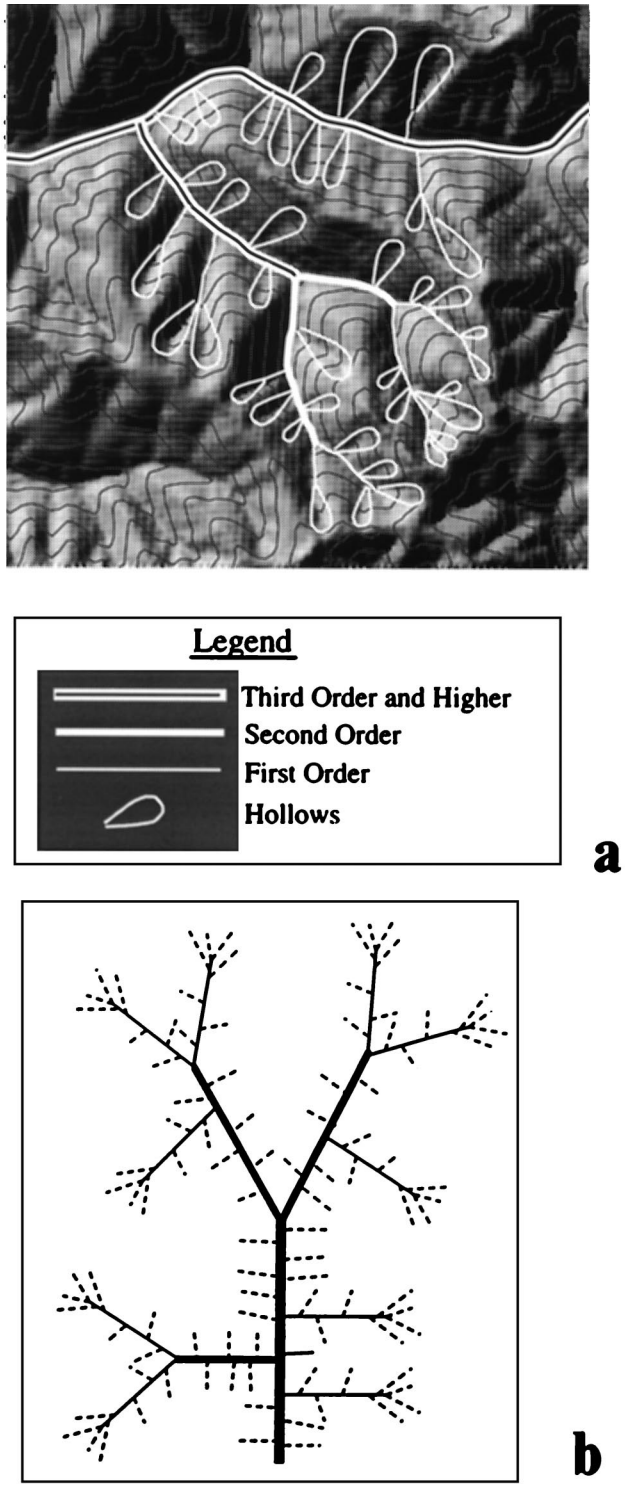


**Figure 2.** (a) Topographic contours and shaded relief showing the bedrock hollow-channel network structure up to third-order in the central Oregon Coast Range (OCR). Landslides in hollows trigger debris flows in first- and second-order channels, which deliver sediment to third- and higher-order valley floors. In addition, some bedrock hollows are located adjacent to third- and higher-order channels. First- and second-order channels comprise about 90% of all channel length in the region. (b) Schematic diagram of the structure of the hollow-channel network in an average 1-km$^2$ area containing a third-order stream (thickest line), three second-order channels (medium lines), 10 first-order channels, (finest lines) and 100 hollows (dashed lines).

years B.P.) of colluvial wedges in the upper parts of nine bedrock hollows to indicate a change in the mid-Holocene climate of the OCR that favored landsliding. *Personius et al*. [1993] established an age of 9000–11,000 years B.P. for an alluvial terrace throughout the central OCR, implying a region-wide evacuation of colluvium from bedrock hollows, presumably brought about by climate change during the Pleistocene-Holocene transition. *Benda and Dunne* [1987] interpreted four basal radiocarbon dates (1600–9500 years B.P.) collected at recent landslide scars in the lower parts of hollows to represent the time necessary to refill landslide scars with colluvium to the point of failure in an unchanging climate. This proposal was not meant to deny the possible role of climatic change but only to admit ignorance in the face of sparse data. *Dunne* [1991] suggested a reconciliation of the differing interpretations of colluvium ages from the upper and lower parts of hollows with a simulation model which suggested that under a steady climate colluvium becomes unstable more frequently in the lower portion of a hollow than in the upper part. Evacuation of the latter may require changes of climate and fire regime of the magnitude proposed by *Reneau and Dietrich* [1990] and *Personius et al*. [1993].

## 3. Climate and Vegetation History

The application of our simulation model to the central OCR is based on the hypothesis that climate of the region has not changed for at least 3000 years. This hypothesis is based on studies of plant pollen assemblages in western Washington State by *Heusser* [1974, 1977], *Barnosky* [1981], *Leopold et al*. [1982], and *Cwynar* [1987], and in western Oregon by *Worona and Whitlock* [1995], indicating that a climate similar to the present one has existed in the OCR for the past 3000–6000 years. *Long*'s [1995] study of pollen and charcoal profiles in a small lake in the OCR suggests no change in fire frequency over at least the past 2000 years, even through the Little Ice Age. The principal reason for climatic stability throughout the mid- to late Holocene in the Pacific Northwest is the moderating influence of the Pacific Ocean and the semipermanence of the north Pacific subtropical high and the Aleutian low that largely control the Pacific coast climate [*Johnson*, 1976].

During the mid- to late Holocene, the humid mountain landscape of the central OCR has been forested predominantly by Douglas fir (*Pseudotsuga menziesii*) and western hemlock (*Tsuga heterophylla*) [*Franklin and Dryness*, 1973] under a climate of rainy winters ($\approx$2200 mm yr$^{-1}$) and dry summers. Wildfires infrequently kill large areas of trees (Figure 3) [*Teensma et al*., 1991; *Agee*, 1993] and control the distribution of forest ages, which range up to more than 200 years [*Andrews and Cowlin*, 1934].

## 4. Stochastic Model of Sediment Supply to a Channel Network

This paper describes a stochastic model for interpreting the roles of temporal and spatial factors that control the sediment influx to channel networks through landsliding and debris flow at the scale of a 215-km$^2$ watershed over thousands of years. We begin by positing a landscape of bedrock hollows linked to a network of channels (Figure 2); the axes of the hollows have probability distributions of gradients and colluvium depths, which are independent of one another as the model begins. Each year, colluvium accumulates in each hollow at rates

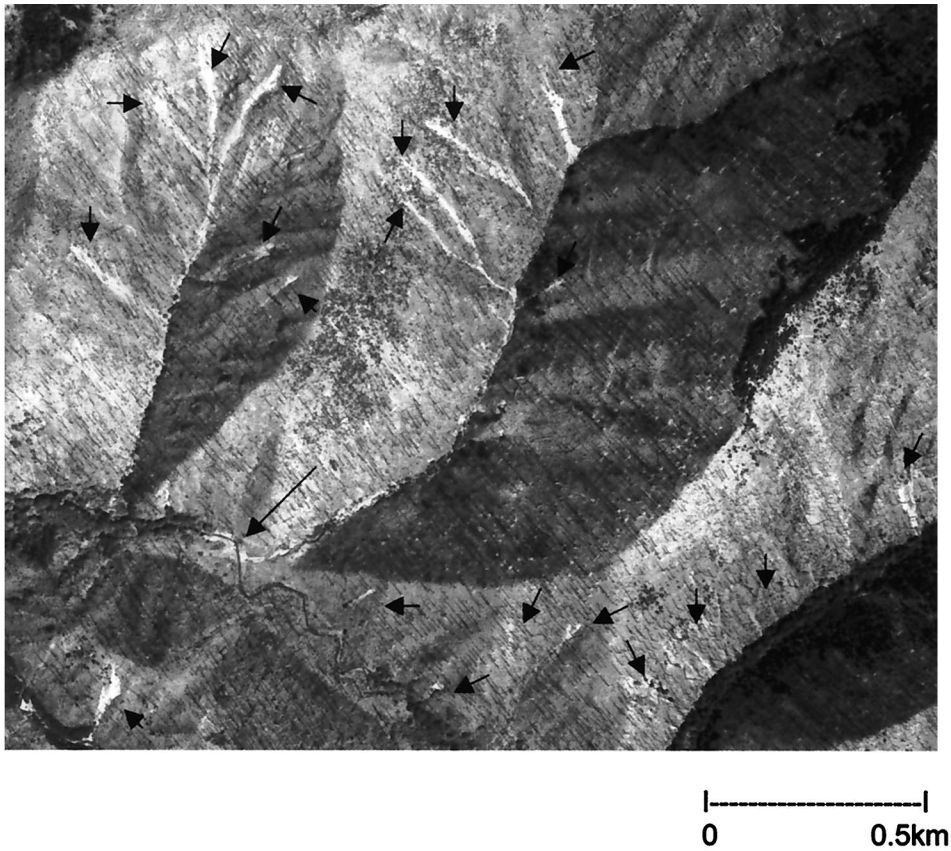


**Figure 3.** Several large and intense fires between 1933 and 1939 in the north-central OCR (the Tillamook fires) led to widespread forest death and the creation of a forest of standing, dead trees in a portion of the Kilchus River basin. Analysis of stereo pairs of 1954, 1:12,000-scale aerial photos revealed a concentration of shallow landsliding in bedrock hollows (small arrows) in the burned area. Some of the failures triggered debris flows in first- and second-order channels (e.g., large arrow) and deposited sediment directly in to a fourth-order channel.

known approximately from field studies, thickening the wedge of colluvium and altering its stability. The population of hollows is subject to a time series of forest fires synthesized randomly from probability distributions of fire location and size typical of the region. After a fire, root strength over a large patch of landscape declines gradually and then begins to recover, causing the strength of the colluvium to evolve through time. A time series of rainstorms synthesized randomly from distributions of intensity and duration generate pore pressures in the colluvium of each hollow, which either fails as a landslide or survives to thicken in succeeding years. The contiguity of burned areas causes spatial concentrations of landsliding (Figure 3), although most colluvial wedges survive a particular fire episode. Depending on its location, each landslide either enters a channel and is deposited or evolves into a debris flow which scours sediment from low-order channels and deposits it downstream. The results include temporal and spatial patterns of sediment pulses emanating from single hollows or groups of hollows, and a continually evolving spatial pattern of forest ages and colluvium depths in the hollows. Computations are summarized in Figure 4.

Results from this stochastic model of sediment supply are used to examine how climate, topography, and spatial scale (drainage area) govern the sediment supply to third- and higher-order channels. In a companion paper [*Benda and Dunne*, this issue] we couple the sediment supply regimes reported in

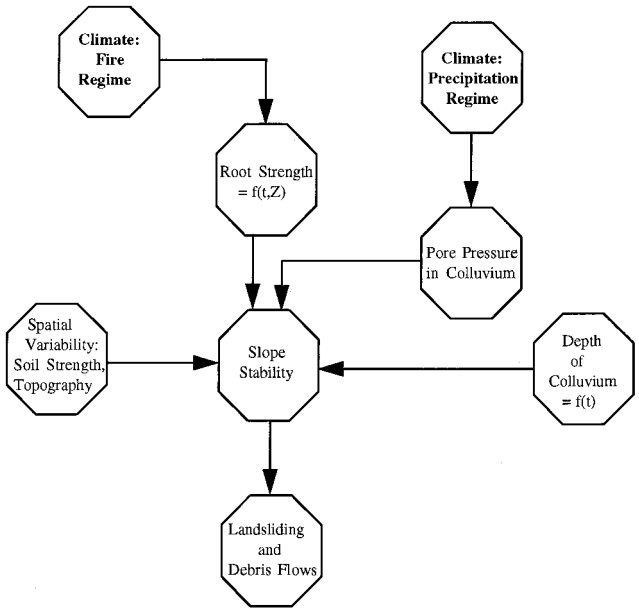


**Figure 4.** Flowchart of the simulation model of the interaction between climatic and topographic conditions that produce landslides and debris flows in the 215-km$^2$ study watershed. The symbols $Z$ and $t$ respectively indicate colluvium thickness and time.

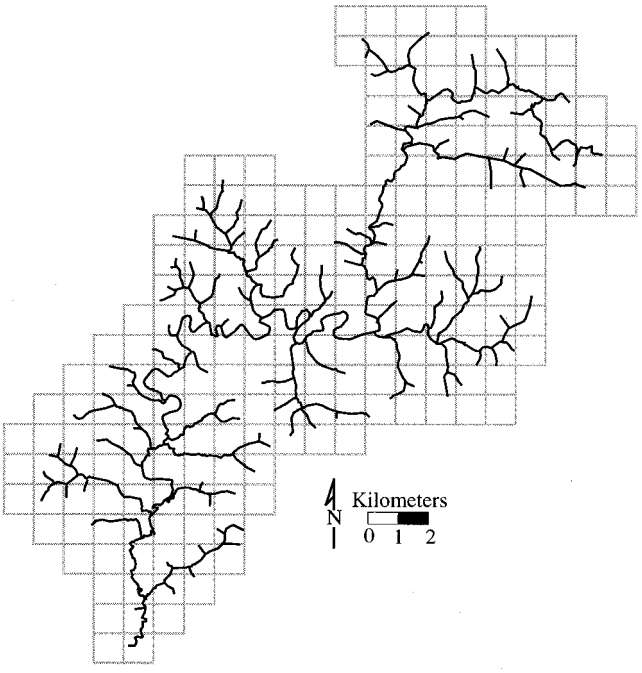


**Figure 5.** The 215-km$^2$ basin of the North Fork of the Smith River divided into square kilometer grid cells for the simulation. The third- and higher-order channel network is also shown.

this paper with a model of sediment routing through a channel network to examine how the hierarchical character of the network, sediment storage in the valley, and the effect of particle abrasion modulate the effects of the stochastic sediment influx from mass wasting to generate the regime of sediment transport and sediment storage over a range of basin size.

### 4.1. Parameterizing the Network Structure of First- and Second-Order Basins

The geometric structure of the network of hollows and channels controls sediment routing by landsliding and debris flow in the OCR [*Benda and Dunne*, 1987; *Benda and Cundy*, 1990]. Bedrock hollows in the region have areas of approximately 0.01 km$^2$, according to our inventories of hollows visible on 1:12,000-scale color aerial photographs of clearcuts in the OCR. They have an average amplitude (from ridge to hollow axis) of approximately 10 m, but are not accurately depicted on 1:24,000-scale topographic maps. Therefore, the zero- through second-order network is represented statistically in our simulation model, rather than being registered spatially. The 215-km$^2$ North Fork basin was subdivided into 1-km$^2$ grid cells (Figure 5), and each cell was assigned 100 hollows. The potential for average cell gradient to affect the spatial density of hollows within cells is ignored. The basin contains 215 grid cells, each with a unique population of 100 hollows that is tracked through time.

The topological relationships between hollows and channels affect sediment routing by landslides and debris flows in any grid cell [*Benda and Dunne*, 1987], and are represented through empirically defined probabilities of sediment transfer between orders (described later and listed in Table 1). The number of first- and second-order channels assigned to each cell is based on the average density of each (10 and 3 km$^{-2}$, respectively) measured from 1:24,000-scale topographic maps after the channel network had been augmented on the basis of aerial photographs and familiarity with the terrain. In the region, two of every three second-order channels (represented schematically in Figure 2b) have three first-order tributaries, the third has two first-order tributaries, and on average two other first-order streams in each grid cell connect directly to third- and higher-order channels. First-order channels are supplied by an average of seven hollows, four being clustered around the channel head, entering the channel at acute angles, and three entering the channel with high junction angles. An average of 6 hollows enters each second-order channel segment, and another 12 intersect higher-order channels in each cell.

**Table 1.** Probabilities of Sediment Transfer to Streams of Various Orders After Landsliding

| Type of Mass Wasting | Transfer Between Sediment Reservoirs | | Probability |
|---|---|---|---|
| | From | To | |
| Landslides | hollow | first-order | 0.30 |
| Landslides | hollow | second-order | 0.18 |
| Landslides | hollow | third- and higher-order | 0.12 |
| Debris flows | hollow and first-order | second-order | 0.08 |
| Debris flows | hollow and first-order | third- and higher-order | 0.08 |
| Debris flows | hollow, first-order, and second-order | third- and higher-order | 0.24 |

The probabilities are derived from the linkages in Figure 2b, and the rules based on field observations and described in the text. The cases are mutually exclusive and exhaustive. The first three involve accumulation of landslide debris in channels, and the others involve the conversion of landslides to debris flows that scour sediment from first- and second-order channels.

### 4.2. Stability Analysis for Colluvial Wedges in Hollows

The geometry of bedrock hollows has been idealized for use in calculations as both a cone [*Humphrey*, 1983; *Iida*, 1984; *Dunne*, 1991] and a tipped, triangular trough [*Dietrich et al.*, 1986]. We approximate the form as a conical hollow that focuses subsurface flow into a narrow wedge of colluvium accumulating in the long, spoon-handle-shaped lower part of the hollow. Colluvium is supplied to this trough between the subparallel lower sideslopes of the hollow by soil creep and associated processes and fails in a long narrow strip. We use the infinite slope model for Mohr-Coulomb failure of root-reinforced colluvium to calculate the stability of the wedge subject to transient pore pressure calculated from a simple model of subsurface flow induced by rainstorms with stochastically varying intensity and duration. Between storms that trigger failure, the colluvium thickens and its root strength changes.

The form of the slope-stability equation used is

$$\mathrm{FS} = \{[C_S + C_L + C_V] + \{[M\gamma_s + (1 - M)\gamma_m - M\gamma_w]Z \cdot \cos^2\theta + T\cos\theta\}\tan\phi\} \cdot \{[M\gamma_s + (1 - M)\gamma_m]Z\sin\theta\cos\theta + T\sin\theta\}^{-1} \quad (1)$$

where FS is the factor of safety (the ratio of shear resistance to gravitational stress); $\gamma_s$, $\gamma_m$, and $\gamma_w$ (kN m$^{-3}$) are the specific weights of saturated and moist colluvium and of water, respectively; $T$ (kN m$^{-2}$) is the weight of trees per unit area; $Z$ (m) is the vertical colluvium thickness; $M$ is the ratio of $h$ (m), the vertical saturated thickness above an impermeable failure

plane (bedrock), to $Z$; $\theta$ is the hillslope angle; $C_S$ (kPa) is the soil cohesion; $C_L$ is the lateral reinforcement contributed by tree roots; $C_V$ (kPa) is the root cohesion exerted by vertical anchoring; and $\phi$ is the angle of internal friction.

### 4.3. Spatial Variability of Hillslope and Soil Mechanical Properties

The geometry of bedrock hollows and the mechanical properties of soils vary spatially in the OCR. Frequency distributions of hillslope gradient and soil depth, friction angle, cohesion, and bulk density of the colluvium are used to represent the spatially variable physical characteristics of hollows in the study basin. Field-measured gradients of hollows ($n = 90$) and colluvium depths at landslide scars ($n = 45$) in the central OCR [*Pierson*, 1977; *Benda*, 1988] were normally distributed with respective means of 38.4° (standard deviation of 4.6°) and 1.0 m (standard deviation of 0.5 m). Estimates for the frequency distributions of soil cohesion ($C_s$), friction angle ($\phi$), and bulk density in the central OCR are obtained from *Schroeder and Alto* [1983]. Their measurements, obtained from four sites in the central OCR, are used to calculate a mean and standard deviation of 38° (±3°) for the friction angle, 0.5 (±0.7) kPa for cohesion, and 11.5 (±0.6) kN m$^{-3}$ for dry bulk density. These properties are assumed to have normal distributions curtailed at zero, and to not vary with soil depth. In addition, hollow geometry and soil mechanical properties are assumed to be independent of each other.

Values for hillslope gradient, soil depth, and soil mechanical properties obtained from the frequency distributions are used in a Monte Carlo simulation to create an initial population of 21,500 bedrock hollows and their associated colluvial wedges distributed across the 215-km$^2$ study basin. Only combinations of physical properties that are stable in the dry state (FS $> 1$) are used. The frequency distribution of FS stabilizes after the simulation of about 100 sites. At the beginning of a model run, each cell holds the same simulated population of 100 hollow gradients and colluvium properties. Thereafter, colluvium depths vary through soil addition (discussed below) and evacuation, and each cell develops a unique population of depths; the other three properties do not evolve.

### 4.4. Accumulation of Colluvium in Hollows

After each landslide, which typically exposes bedrock, colluvium refills the scar and thickens over millennia, gradually changing the relative magnitudes of gravitational and frictional forces and root reinforcement [*Sidle*, 1987, 1992; *Dunne*, 1991]. Soil creep, tree throw, animal burrowing, and small landslides transport colluvium from hillslopes to bedrock hollows (and to channels). These processes can be represented as continuous transport over long periods, and *Reneau and Dietrich* [1991] used radiocarbon dating of colluvium to estimate transport rates of 11–90 (average 32) cm$^3$ cm$^{-1}$ yr$^{-1}$ into bedrock hollows in the OCR.

We applied a single average rate of soil accumulation in each of the 21,500 hollows based on soil entering each side of a representative trough-shaped landslide scar obliquely at an angle averaging 29° [*Reneau and Dietrich*, 1991]. Each centimeter of trough length therefore fills at $dV/dt = 2 \times \sin 29° \times 32$ cm$^{-3}$ cm$^{-1}$ yr$^{-1}$ (= 31 cm$^3$ cm$^{-1}$ yr$^{-1}$). The representative scar was assumed to have a bottom width ($w_b$) of 4 m and sideslope angles ($\psi$) of 35°, based on our field observations, and therefore to fill as a quadratic function of time in years since evacuation ($t$):

$$Z(t) = [(w_b^2 + 4 \cot \psi V(t))^{1/2} - w_b] \frac{\tan \psi}{2} \quad (2)$$

### 4.5. Temporal Variation in Root Reinforcement

Roots of trees and shrubs reinforce soils laterally and bind thin soil to partially fractured bedrock. This reinforcement decreases as soil thickens or as roots die after intense wildfires, and it increases as roots recolonize a soil after fire. Studies in timber harvest sites have shown that roots decay after the death of vegetation, and the effective cohesion of the soil declines [*Burroughs and Thomas*, 1977; *O'Loughlin and Watson*, 1979; *Ziemer*, 1981]. Although we are not aware of published studies of the loss of root strength following wildfires in humid forests of the Pacific Northwest, aerial photographs of burned forests in the north-central OCR reveal concentrated landsliding from bedrock hollows following forest death and root decay (Figure 3). Therefore we accept as reasonable the proposition and evidence summarized by *Swanson* [1981] that death of vegetation by forest-replacing wildfires has an effect on slope stability similar to that of timber clearcutting in the OCR.

Little is known about the partitioning of root strength between lateral reinforcement and vertical anchoring by roots that penetrate bedrock fractures. For the purpose of illustration of how such a partitioning might affect the frequency of landsliding, *Dunne* [1991] suggested the separation of the maximum apparent root cohesion into the sum of a lateral root cohesion and a vertical root cohesion He suggested that under mature forest the effectiveness of vertical anchoring would diminish as soil depth increased according to

$$C_{VM} = \text{MVRC} \exp(-jZ) \quad (3)$$

where $C_{VM}$ (kPa) is the apparent cohesion under mature forest due to vertical anchoring by roots, MVRC (kPa) is the maximum vertical root cohesion, $Z$ (from equation (2)) is the vertical colluvium depth along the axis of the hollow, and $j$ is set to 2 m$^{-1}$, based on field observations in the OCR that anchoring approaches zero for soil depths greater than 1.5 m. For purposes of illustration, we use a total root cohesion of 14 kPa obtained from measurements in the OCR by *Burroughs and Thomas* [1977], and values for MVRC and maximum lateral root cohesion (MLRC) that are, respectively, 30% and 70% of this figure, as estimated by *Hammond et al*. [1992] from a comparison of the role of root strength in the infinite-slope model and in *Burroughs*' [1984] 3-D block model of failure.

To simulate the loss of rooting strength following wildfire, the model of *Sidle* [1992] is used in which root decay follows a negative exponential curve, and the subsequent increase in root strength due to new forest growth follows a sigmoid curve. Root decay is represented by

$$D = \exp(-k\tau^n) \quad (4)$$

where $D$ is the dimensionless relative reinforcement during decay (actual strength divided by maximum strength), $k$ (= 0.5 yr$^{-1}$) and $n$ (= 0.73) are constants derived from measurements by *Burroughs and Thomas* [1977] in Douglas fir forests of the OCR, and $\tau$ (years) is the time since forest death. The sigmoid root-growth curve proposed by *Sidle* [1991] is written as

$$R = [a + b \exp(-f\tau)]^{-1} + c \quad (5)$$

where $R$ is the dimensionless relative reinforcement due to regrowth, and $a$, $b$, $c$, and $f$ are empirically derived constants

having values of 0.95, 19.05, −0.05, and 0.25 $yr^{-1}$, respectively, as derived by *Sidle* [1992]. The sum of $R$ and $D$, which cannot exceed 1.0, gives the combined relative root reinforcement in any year following forest demise and is multiplied by the sum of MLRC and MVRC to predict root cohesion ($C_V + C_L$ in equation (1)) in any year:

$$C_V + C_L = (D + R)[\text{MVRC} \exp(-jZ) + \text{MLRC}] \quad (6)$$

The result is a curve with a minimum value, based on the chosen parameters, of 0.3 kPa between 4 and 8 years after widespread tree death.

Incorporating recent studies of processes that control root-strength changes introduces eight parameters in (4)–(6), which is an unfortunate escalation of data requirements. For illustrating stochastic forcing of sediment supply, we could have replaced these equations with simpler combinations of linear trends without significant loss of detail, but we chose to incorporate the complexity to highlight current process-based research on root reinforcement that might reduce uncertainty in one module of a system approach such as the one we are illustrating. Other applications might require only a simple expression for root strength that contains a minimum of 4–10 years after tree death.

Although mass wasting from bedrock hollows of steep, humid landscapes can result from a self-driven cycle of colluvium accumulation and failure during rainstorms when the soil reaches a critical thickness under dense forest (as $C_v$ in (6) declines) [*Hack and Goodlett*, 1960; *Dietrich and Dunne*, 1978; *Okunishi and Iida*, 1981], many landslides and debris flows in the OCR follow vegetation death by wildfires when root strength is lowest [*Swanson*, 1981, Figure 3]. To represent this effect in our model of the spatial and temporal patterns of landsliding, we simulated the frequency, size, and spatial distribution of forest-replacing wildfires in the North Fork Smith River basin and computed the effect on root reinforcement in each grid cell using (6).

The spatial and temporal occurrence of stand-replacing forest fires was predicted by applying the fire model of *Agee and Flewelling* [1983], which calculates an annual ignition probability for a square kilometer on the basis of local climatic records of droughts and thunderstorms. The model then randomly selects a burned area from an exponential probability distribution of fire sizes [*Teensma*, 1987] with a mean of 30 $km^2$, based on fire history in the OCR [*Benda*, 1994]. The fire is positioned in the landscape with a random number generator and a flammability index controlled by the age of the forest in each cell (highest for ages <20 years; least for ages 50–150 years; higher for >150 years) [*Agee and Huff*, 1987]. The fire burns in a radial pattern in increments of 1 $km^2$, leaving 30% of the cells in unburned islands to simulate unsuccessful fire transmission because of local moisture and topographic conditions [*Isaac and Meagher*, 1936]. The resulting long-term average fire frequency at a point was 1/250 years. In a stratigraphic study of charcoal deposits in a 9000-year-old lake core from the OCR, *Long* [1995] found that fire regime has remained relatively constant for the last 3500 years, and during that time interfire periods, based on charcoal deposits, ranged from 175 to 300 years.

The highest probability of ignition in the model occurs during the 20 years following a fire, when there is an abundance of dead and dying organic material available for burning, and back-to-back fires create the lowest root strengths. Fire intensity is not considered explicitly in the model. Possible effects of topography on fire spreading which would add another variable element in the erosion regime [*Benda et al.*, 1997, Figure 5] are not included because of the lack of field data on this topic in the OCR. The initial distribution of forest ages in the basin at the beginning of a model run is exponential with a mean equal to the fire recurrence interval, which is equivalent to the average long-term forest age structure [*Van Wagner*, 1978; *Agee*, 1993].

### 4.6. Pore Pressures in Bedrock Hollows

The convergent topography of bedrock hollows concentrates subsurface flow, increasing pore pressure (and therefore $M$ in (1)), and reducing the stability of the colluvial wedge. The thickness of the colluvium saturated by a storm depends on the geometry of the hollow, the hydraulic conductivity of the colluvium and of any underlying fractured bedrock [*Wilson and Dietrich*, 1987; *Montgomery*, 1991], the antecedent moisture in the colluvium, and the intensity and duration of the storm. A simple model of subsurface flow in hollows is used to illustrate the general principle of how topography affects pore pressure. An analytical solution for flow through a uniform soil in a conical depression supplying water to the linear colluvial wedge [*Humphrey*, 1983; *Iida*, 1984] requires constant rainfall intensity, saturated hydraulic conductivity, unfilled porosity at the beginning of each storm, and no change in storage within the unsaturated zone. *Dunne* [1991] used this approach to derive the peak saturated thickness ($H$) following a storm of intensity ($I$) and duration ($T$) along any horizontal radial distance ($x$):

$$H = Ix(R - 0.5x)/K \sin\theta(R - x) \qquad x < x_s \quad (7)$$

$$H = Ix_s(R - 0.5x_s)/K \sin\theta(R - x) \qquad x > x_s \quad (8)$$

$$x_s = K \sin\theta \cos\theta T/p \quad (9)$$

where $x_s$ is the radius downslope of which runoff can attain steady state during the storm. In these equations, $K$ is the saturated hydraulic conductivity, taken as 0.4 m $hr^{-1}$ [*Harr*, 1977; *Montgomery*, 1991]; $p$ is the unfilled porosity of the colluvium, taken as 0.4 [*Hough*, 1957]; $\theta$ is the steepness of each cone; and $R$ is the radius of the cone (150 m, the mean value for the region and lithology). The value of $M$ in (1) is then calculated using

$$h = H/\cos\theta \quad (10)$$

Since we are concerned only with illustration of how fire and rainstorm control spatial and temporal clustering of erosion, we did not calculate pore pressure and slope stability for all points within the hollow [*Dunne*, 1991] but for a single radial distance of 50 m, which is included within almost all observed failures in the area.

Time series of rainstorm intensity and duration are generated from a stationary stochastic process in which both $I$ and $T$ of individual storms are independently distributed according to exponential density functions [*Eagleson*, 1972; *Beven*, 1987]:

$$f(I) = \left[\frac{1}{M_I}\right] \exp(-I/M_I) \quad (11)$$

and

$$f(T) = \left[\frac{1}{M_T}\right] \exp(-T/M_T) \quad (12)$$

where $f(\ )$ denotes the probability density function, $M_I$ is the mean storm intensity, $M_T$ is the mean storm duration, and the mean annual rainfall is $(M_I \times M_T)$. The largest storm of each year is used to estimate $H$ in (8) and therefore $M$ in (1). Although interarrival times of storms and antecedent conditions are undoubtedly important in some landslide triggering storms, these aspects of hillslope hydrology are not included in our model. A mean intensity of 1.7 mm $hr^{-1}$ and a mean duration of 20 hours are used in (11) and (12) on the basis of hourly rainfall measurements within the study watershed during years 1989–1991.

A total of 62 storms is predicted each year based on a mean annual precipitation of 2200 mm; only the largest storm of each year is used to calculate saturated thickness of soil and slope stability. Because precipitation intensity and duration are approximated as being independent of each other, estimates of probable maximum precipitation [*U.S. Weather Bureau*, 1960] are used to limit total rain depth. Intensity and duration of these large frontal storms are assumed to be spatially uniform across the 215 $km^2$ area of the calculation, although individual rainstorms in the region presumably have characteristic spatial dimensions, adding another spatial element to the occurrence of landsliding that is not treated here.

### 4.7. Sediment Supply From Landsliding

The average volume of a landslide that originates from a hollow in our model is governed by the amount of colluvium that accumulates during an average interlandslide period within a space defined by the geometry of a landslide scar. In order to reduce the computational load and to ignore complications such as secondary failures [*Lehre*, 1982], we used an average landslide volume of 1200 $m^3$, which would result from the average depth at which the colluvium becomes unstable (1.5 m), the typical scar cross section used in (2), and a scar length of 125 m. We did not calculate the variable lengths of failures that would result from variation in failure history and storm size through the simulation [*Dunne*, 1991]. The result of this simplification was only to reduce the temporal variability of the sediment input to channels, minimizing the stochastic effect.

The colluvium evacuated from hollows by landsliding follows one of several pathways prior to its deposition in third- and higher-order channels based on a routing model that uses hollow-channel network structure [*Benda and Dunne*, 1987; *Benda and Cundy*, 1990]. The diversity of sediment routing pathways in the study basin has been defined by field studies [*Benda and Dunne*, 1987]. First, colluvium from landslides and soil creep (supplied at 32 $cm^3\ cm^{-1}\ yr^{-1}$, as referred to above) may become stored in first- and second-order valley floors until scoured downstream by a debris flow. Second, landslides can trigger debris flows that travel through first- and second-order channels and deposit sediment directly into third- and higher-order channels or onto debris flow fans and terraces. Third, soil creep and landslides adjacent to higher-order channels may contribute sediment directly to those channels.

### 4.8. Debris Flow Sediment Transport in First- and Second-Order Channels

Most of the sediment delivered to first- and second-order channels in the central OCR originates from landslides and debris flows. The thick, armored, and tree-reinforced sediments resist fluvial erosion and accumulate until scoured by episodic debris flows [*Benda and Dunne*, 1987]. Between debris flows, landslides and soil creep contribute colluvium to channels, and fluvial erosion removes an average of 20–30% of the long-term sediment supply [*Swanson et al*., 1982; *Benda and Dunne*, 1987; *Benda*, 1988; *O'Connor*, 1994], and therefore the magnitude of the accumulation available for scour by debris flow depends primarily upon the amount of time elapsed since the previous debris flow.

The routing of sediment by landslides and debris flows between the hillslope and channel storage reservoirs is based on hollow-channel network structure defined by tributary junction angles and channel gradients [*Benda and Dunne*, 1987]. In a typical drainage network in the region (Figure 2b), three hollows typically join the first-order segment approximately at right angles and four others are clustered around the head of the channel, allowing debris flows to enter it at acute angles and to continue downstream. *Benda and Cundy* [1990] showed that a channel junction angle of less than 70° was required to allow the flow to proceed in this region. If the angle was higher, the debris flow collided with the wall of the receiving valley and came to rest, adding a charge of debris to the sediment stored in the first-order channel. Similarly, debris flows passing through first-order channels continue to flow along the second-order channel only if the junction angle was less than 70°; in the field this occurred at the junction which created the second-order segment, but the third first-order segment in a typical second-order basin usually entered at right angles, and hence debris was deposited at that location. When a debris flow did not encounter any high-angled confluences, all colluvium was scoured from first- and second-order channels along its path, and deposition of the original landslide and the scoured colluvium occurred in third-order segments where channel angles decreased to 3.5°.

This topological model of landslide and debris flow sediment routing, when applied to a typical grid cell (Figure 2b) that contains 100 hollows and 10 first- and 3 second-order channels, expresses the transfer of colluvium by landslide and debris flow, in terms of probabilities (Table 1). The number of landslides in each grid cell in a year is first predicted. Then transfer probabilities, calculated from the number of possible transfer paths in Figure 2b, which is assumed to characterize each cell, are used to determine how sediment moves through the network to third- and higher-order channels (Table 1). When a debris flow passes through a first- or second-order segment, all colluvium that has accumulated there since the previous debris flow is transported downchannel. The results include a time series of sediment delivery to each third- and higher-order channel in the network and a running tabulation of sediment storage in each hollow and first- and second-order channel in the third-order basin.

### 4.9. Summary of Model Operation

The following sequence of operations occurs in the stochastic model when it is applied to the 215-$km^2$ North Fork of the Smith River basin. A population of 21,500 bedrock hollows with variable steepness is generated and is assigned a randomly synthesized population of colluvial wedges with a distribution of initial depth, cohesion, friction angle, and bulk density. Each year, the colluvium depth ($Z$) in the axis of each bedrock hollow (equation (2)), and similarly in each channel segment, increases through supply by soil creep. Wildfires of random location and size kill a proportion of the forest in the basin, resetting the forest age in the affected cells, and initiating root decay. Root cohesion ($C_L$, $C_V$) is updated annually in re-

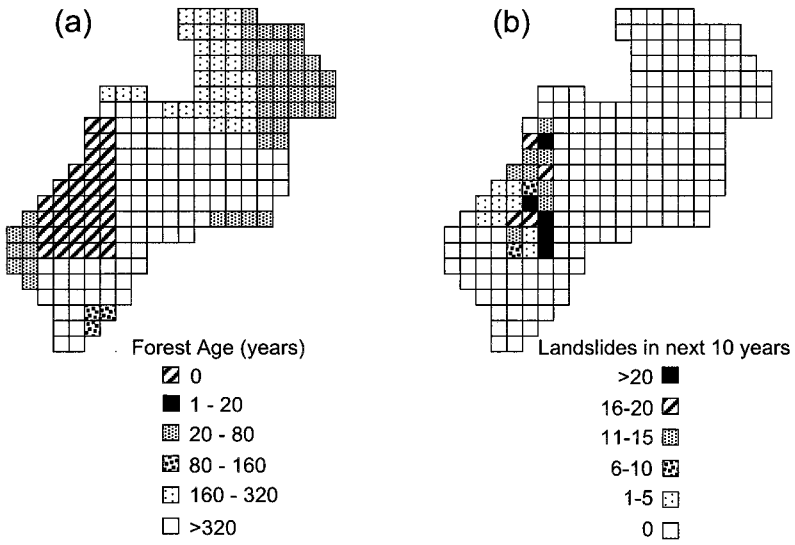


**Figure 6.** (a) Model predictions of forest ages in the 215-km$^2$ study basin in year 2534 that resulted from the previous four centuries of wildfire history. A 33-km$^2$ fire (forest ages <1) occurred in year 2534. (b) The corresponding spatial distribution of the number of landslides that occurred in the first decade following the fire. The number of landslides in grid cells is variable, despite the uniform treatment by fire and precipitation over the 33 km$^2$, because each square kilometer of the basin has already developed a unique frequency distribution of colluvium thicknesses in bedrock hollows as a result of the nonuniform occurrence of wildfires in the previous 25 centuries of model simulation. In other years of the simulation, landslides also occur outside of recently burned areas, but not in year 2534. Ninety percent of slides are predicted to occur during 20-year periods following fire.

sponse to the changing forest age and soil depth in each hollow (equation (6)). The intensity and duration of the largest storm of each year is calculated from (11) and (12), and used in (7)–(10) to compute saturated vertical thickness ($h$) in each bedrock hollow. Then the factor of safety is calculated for each of 100 hollows in each square kilometer using (1). The number of hollows with factor of safety <1 is used to calculate the annual failure rate for each grid cell (number of failures/100 hollows). The transfer of colluvium between hollows and the channel network, and therefore the number and volumes of debris flows, are calculated by applying the sediment transfer probabilities in Table 1.

## 5. Simulation Results

Figure 6 is a sample model prediction for simulated year 2534 showing the location and size of a fire in the 215-km$^2$ North Fork basin (forest age <1 year), the diversity of forest ages resulting from earlier fires, and landsliding rates in the succeeding decade. Because the filling of landslide scars to a depth at which they are likely to fail requires millennia and because the interarrival times of fires and storms are only centuries and decades, respectively, the antecedent history of fire and storm affects mass wasting rates. Each hollow develops a unique soil depth as a result of its particular history of fire and storm in preceding centuries, and landslide rates vary within the recently burned area because of this spatial variability in antecedent conditions (Figure 6b). However, the frequency distribution of colluvium depths over the whole basin stabilize rapidly during the simulation. Landslides occur outside of recently burned areas in other simulated years, but with the parameter values that we and others have judged to be reasonable, as outlined above, 90% of all simulated slides occur in areas that have burned within the preceding 20 years.

### 5.1. Frequency and Distribution of Landsliding in Bedrock Hollows

The long-term frequency of landsliding in bedrock hollows is controlled by the rate of colluvium production, a geological and climatic influence represented by the average colluvium supply rate of 32 cm$^3$ cm$^{-1}$ yr$^{-1}$ to the hollow axis [*Reneau and Dietrich*, 1991], which governs accumulation along the hollow axis and changes the balance of gravitational force and root strength in the colluvial wedge. Over shorter timescales the occurrence and intensity of wildfires and rainstorms concentrate the sediment supply to channels in ways that depend mainly on the probability and size of forest-replacing wildfires; the intensity, duration, and spatial scale (not treated here) of rain storms; and the geometry of hollows that control the slope-stability relations in (1) and the size of scars reflected in (2).

The interarrival times of landsliding in the 21,500 bedrock hollows (Figure 7) varied between 500 and 4000 years and averaged approximately 2500 years, during model runs of 8000 years. According to (2), such a range of timing should result in a range of colluvium depths from 0.4 to 2.2 m, which is close to that measured at landslide scars in bedrock hollows on the same lithology in the region: 0.6–1.6 m with a mean of 1.0 m [*Pierson*, 1977] and 0.4–2.0 m with a mean of 1.3 m [*Benda*, 1988]. *Reneau and Dietrich* [1991] measured a depth range of 1.3–4.2 m with a mean of 2.7 m in colluvial wedges that were mainly near the upper ends of hollows. There are too few documented ages of colluvial wedges available from the past 3000 years for the construction of a frequency distribution of landslide interarrival times, and even the ages that yielded the average colluvium supply rate used here are derived from sites that may have experienced subtle changes of climate and fire regime [*Reneau and Dietrich*, 1990]. In this paper, however, our

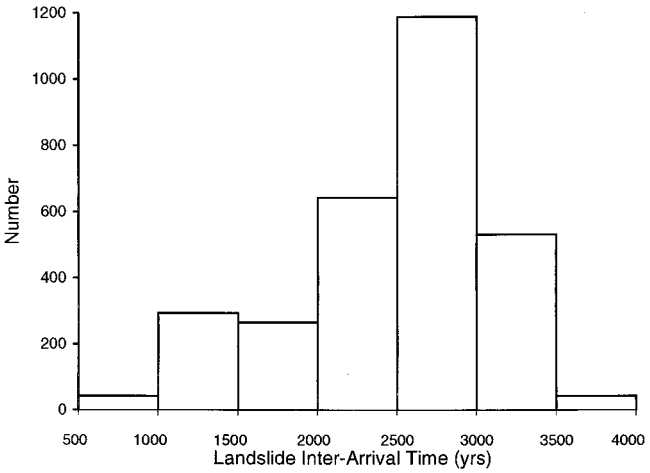


**Figure 7.** Frequency distribution of predicted interarrival times of landslides in the 21,500 bedrock hollows in the 215-km$^2$ basin. The average interarrival time is 2500 years during model runs of 8000 years. According to the field-derived input parameters for this simulation, the depth of colluvium that would accumulate in the hollow during the range of landslide interarrival times of 500 and 4000 years is between 0.4 and 2.2 m.

emphasis is on the general principle of how the spatial and temporal patterns of sediment supply are controlled, regardless of the average rate.

### 5.2. Frequency, Volume, and Distribution of Debris-Flow Erosion in First- and Second-Order Channels

Variation in the location and timing of wildfires over thousands of years ensures that each of the 2795 first- and second-order channel segments has a unique time series of sediment storage and therefore debris-flow volumes, yet the long-term statistical properties of these volumes are similar among all channels of a given order. Figure 8 illustrates the process of infrequent debris-flow erosion and sediment storage in one first- and one second-order channel segment, respectively 250 and 300 m in length, during an 8000-year simulation. The instantaneous decreases in sediment storage represent debris flows in first- and second-order channels that are triggered by landslides originating in bedrock hollows (a process controlled by the hollow-channel geometric structure illustrated in Figure 2). In the model and the field area, debris flows erode all of the colluvium stored in first- and second-order channels between flows. The gradual increases in sediment storage following a debris flow represent the net effect of soil creep and fluvial erosion. The abrupt increases in sediment storage of 1200 m$^3$ (vertical increments in Figure 8) are caused by landslides from hollows that contribute colluvium to low-order channels, and the larger vertical increases in Figure 8b indicate sediment scoured from first-order tributaries and deposited in second-order channels. The clustering of erosive debris flows and landslides that contribute colluvium to the channel reflect a general weakening of root strength in part of a basin for a period of years following a wildfire. Consequently, the sediment mass balance of first- and second-order channels fluctuates greatly over periods of a few years.

Periods between debris flows in the first-order channel ranged between 100 and 1300 years (average 600 years), resulting in debris-flow scour volumes of 300–3000 m$^3$. Interarrival times of debris flows in second-order channels ranged between 200 and 1600 years (average 300 years), and debris-flow scour in the second-order channel segment ranged from 200 to 9000 m$^3$. To predict the average volume of a debris flow at the mouth of a first-order basin, the average landslide volume of 1200 m$^3$ is added to the average debris-flow scour of approximately 1000 m$^3$ for a total of 2200 m$^3$. Debris flows that evacuate sediment from second-order channels always travel through first-order channels, and therefore the average volume of debris flows at the mouth of second-order basins is the sum of the triggering landslide and combined scour volumes from first- and second-order channel segments. The average volume of debris flows at the mouths of second-order channels is approximately 6000 m$^3$.

The frequency distributions of sediment volumes stored in typical first- and second-order channel segments at the end of each year during the 8000-year simulation are shown in Figure 9. In the first-order channel (Figure 9a), the mode (0–500 m$^3$), representing about 40% of all years, reflects time periods when sediment accumulates by soil creep following a debris flow but before any landslide contribution. Presumably, fluvial erosion in times of gradual additions of sediment is more efficient than after catastrophic additions, so in these years, the low-order channels may have even smaller accumulations than indicated in Figure 9a. The secondary and tertiary modes in the distribution (i.e., 1000–1500 and 2500–3000 m$^3$) represent the addition of one and two contributing landslides from bedrock hollows to the channel sediment store. The probability of larger accumulations prior to a scouring debris flow is low because the interarrival time of debris flows limits accumulation periods. The frequency distribution of sediment volumes in a second-order channel is similarly shaped (Figure 9b), although larger accumulations also result from the addition of debris flows (originating from the third first-order tributary in each second-order basin shown in Figure 2b).

### 5.3. Frequency and Magnitude of Landsliding at the Basin Scale

The frequency, magnitude, and location of landsliding and debris flows control the spatial and temporal pattern of sediment supply to higher-order channels. The rate of landsliding in grid cells is variable and depends on the history of failures triggered in this case by fires and storms. For example, in years (and cells) in which landsliding occurred, the failure rate (number of landslides per year out of the 100 hollows in a cell) varied between 1 and 50 failures out of 100 hollows per cell with a mean of 6 in a 3000-year simulation for the 215 km$^2$ basin (Figure 10). Simulated failure rates per fire episode (defined as the 20-year period following a fire) are also right skewed with a mean of 15 (Figure 11). In 6- to 12-year aerial-photograph records and field inventories after clearcutting in the OCR [*Swanson et al*., 1981; *Ketcheson and Froehlich*, 1978; *Gresswell et al*., 1979; *Bush*, 1983], annual landslide rates range from 1 to 2 and episode failure rates ranged between 10 and 13 (excluding landslides associated with roads) [*Benda*, 1994]. Aerial photographs after the Tillamook fires (e.g., Figure 3) indicate rates of 30 or more per 100 hollows that can be observed after a sequence of intense fires.

The number of potential landslide sites (bedrock hollows), the probability of storms intersecting recent fires, and hence the frequencies of landsliding increase with increasing basin area. Landsliding in a single hollow is a relatively rare event, occurring on average once every 2500 years. In a third-order

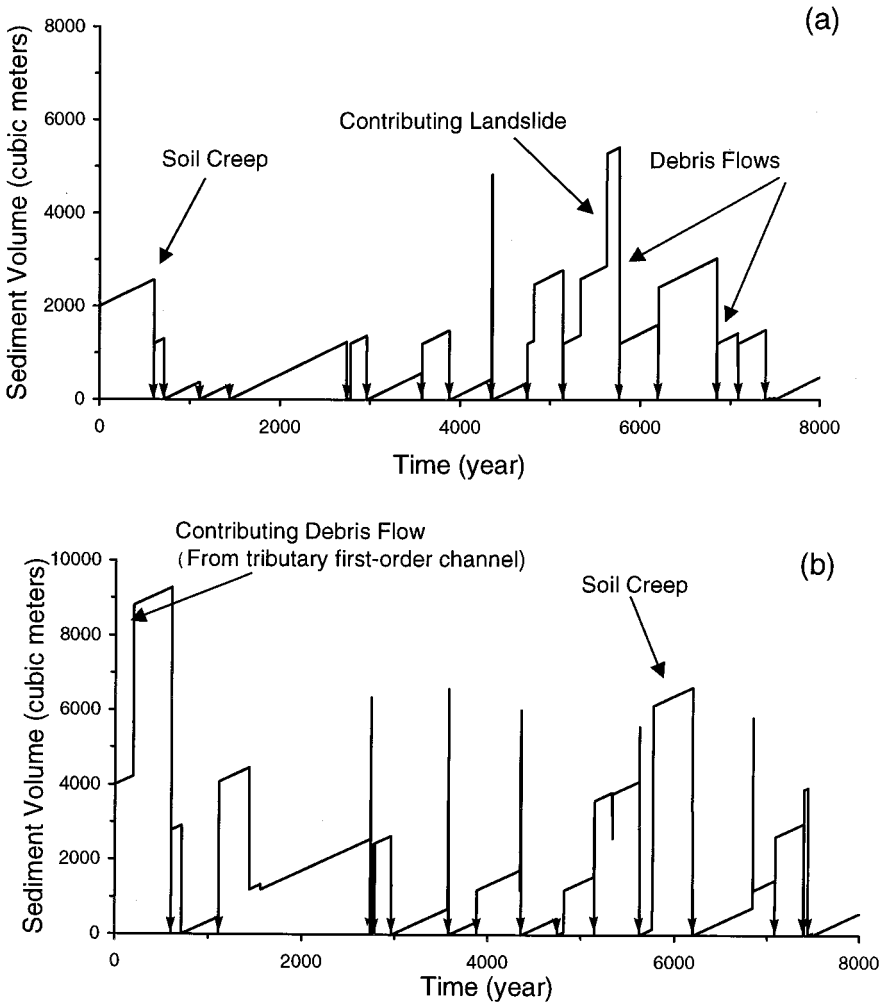


**Figure 8.** (a) Predicted time series of sediment stored in a typical first-order channel over a period of 8000 years. Instantaneous decreases to zero in sediment storage (downward pointing arrows) represent debris flows triggered by landslides in bedrock hollows (a process controlled by hollow-channel network topology). Gradual increases (sloping lines) in sediment storage are the net result of soil creep and fluvial erosion. Abrupt increases in sediment storage of 1200 $m^3$ are caused by landslides that contribute sediment to the channel. (b) Predicted time series of sediment stored in a typical second-order channel over a period of 8000 years. Processes of debris flow scour, soil creep, and landslides are similar to those in first-order channels (Figure 8a). The larger (>1200 $m^3$) increases in sediment storage in Figure 8b are the result of debris flows that scour sediment from a first-order tributary and deposit it in the second-order channel. Both accumulation of landslide debris and scouring by a debris flow occur in the reach in some years, resulting in sharp spikes in storage or decreases that appear to not go to zero. Not all scouring debris flows are shown; some arrows represent multiple debris flows closely spaced in time, particularly in the second-order channel.

basin of 3 $km^2$ the frequency of landsliding increases to about once every 200 years (range: 100–1000 years), and the magnitude of pulses of sliding increases to 1–13 slides per fire episode (Figure 12a). As basin size increases to 25 $km^2$, the frequency of landsliding increases to once every 50–100 years (ranging from a few years to a few centuries), and the magnitude of landsliding increases to 5–165 slides per fire episode (Figure 12b). At a drainage area of 215 $km^2$ (Figure 12c) the frequency of landsliding in the watershed increases to almost once per decade and the number of landslides during fire episodes increases to 10–550.

Approximately 90% of landslides predicted by the model follow wildfires when root strength is reduced, and hence although slides may be distributed widely after a particularly large storm, they typically clump persistently for some years within a fire boundary (Figures 3 and 6). Only a small portion of all landslides are triggered by rainstorms alone because the likelihood of creating the necessary thick colluvial wedges (approximately >1.5 m) that would fail under intact forest canopy is small when the average interarrival time of forest-replacing fires is 250 years and the time required to create colluvium thicker than 1.5 m exceeds 2500 years.

The model predictions of frequency and magnitude of landsliding illustrate some relationships between disturbance frequency and size and basin area. In this case the dominant disturbance is stand-replacing fires, and the secondary disturbance is a rainstorm. If the basin area is smaller than or equal to the size of most fires (such as in the case of the 3 $km^2$ basin in Figure 12a), then frequency of landslide episodes is similar to the frequency of fires. If the basin is larger than commonly

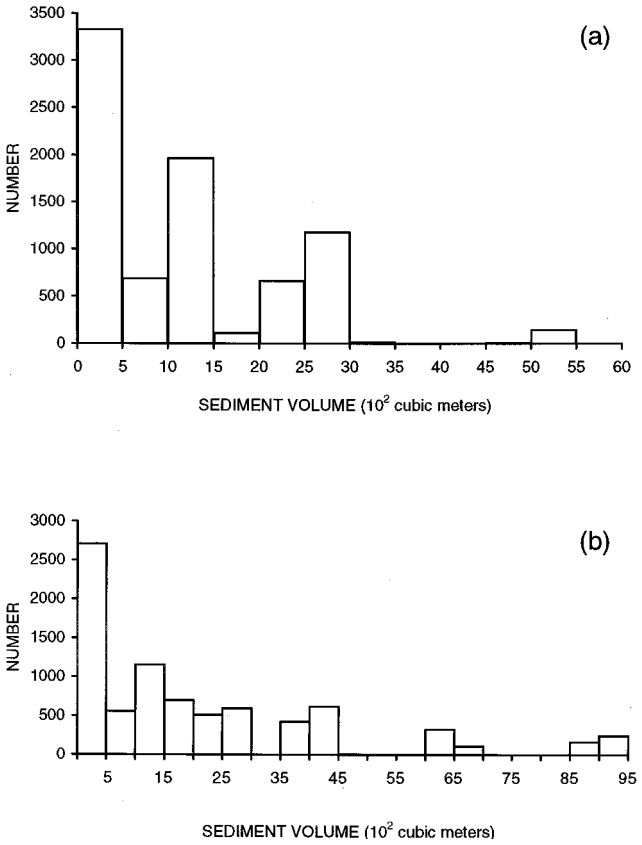


**Figure 9.** Predicted frequency distribution of sediment volumes in (a) first-order and (b) second-order channels over a period of 8000 years.

occurring fires, landsliding frequency will increase at the rate at which vegetation-disturbance events increases with basin area and therefore will depend on the ratio of basin size to average fire size (for the case we have chosen in which storms are uniform across the basin and all stand-replacing fires are of equal severity). The erosion magnitude (number of slides in an episode) is controlled by the density of potential landslide sites, disturbance size, and severity (in this case of the rainstorm, since we have treated all stand-replacing fires as being equal in the severity of root destruction), and time since last disturbance (which allows colluvium to accumulate and which reflects antecedent storm and fire history).

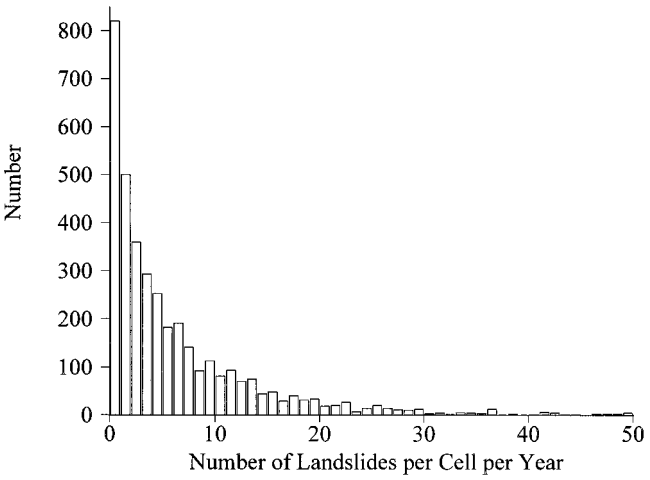


**Figure 10.** Frequency distribution of annual landsliding rates (number of slides/100 hollows) predicted by the model in years and cells with one or more landslides. The annual failure rate ranged between 1 and 50 landslides per cell and averaged 6.

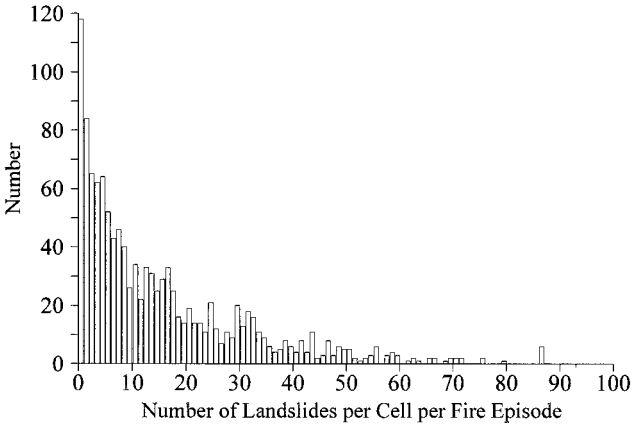


**Figure 11.** Frequency distribution of landsliding rates (total number of landslides/cell) in fire episodes (defined as a 20-year period following a fire). Fire episode failure rates averaged 15 landslides per cell.

## 6. Conclusion

The frequency, magnitude, and spatial distribution of sediment influx to channel networks are stochastic characteristics, which can be analyzed as the results of interactions among topography and climatic and biotic processes, and therefore that vary between regions in nature and intensity. Application of this principle to a 215-km$^2$ drainage basin in the central OCR allows one to analyze expected patterns of sediment influx from mass wasting in terms of (1) a deterministic colluvium supply to bedrock hollows and to channels of all orders, (2) a stochastic sequence of stand-replacing wildfire (determining its timing, size, and location), (3) a stochastic sequence of rainstorm intensity and duration, (4) the resultant effects on hillslope hydrology and the stability of colluvial wedges, and (5) the effects of the hollow-channel network structure on scour and deposition by debris flows. These interactions generate temporal and spatial patterns of sediment supply to channel networks, and the patterns vary systematically with drainage basin size. There is room for incorporating into the analysis the stochastic influences of storm size and location, fire intensity, and geomorphic characteristics such as hollow convergence angles and colluvium production rates, but we have ignored these effects because of lack of data and in order to avoid obfuscating any further our central principle concerning the stochastic forcing of sediment delivery. Our primary objective is to highlight the relationships between large-scale properties of landscapes and the long-term stochastic behavior of erosion and sediment supply.

Hypotheses generated by the model include that there are right-skewed frequency distributions of sediment depth and age in hollows and in first- and second-order channels within a region. Furthermore, one should be able to relate interregional differences in these distributions to differences in climate, land-cover history (including the effects of fire, land

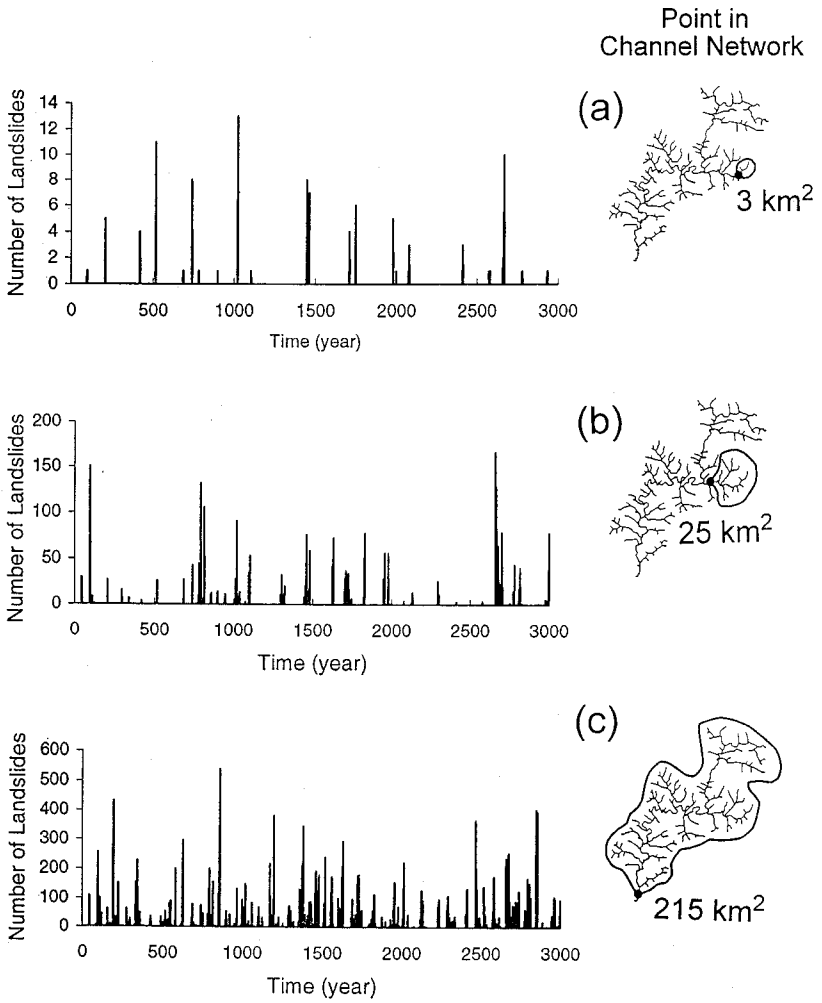


**Figure 12.** Frequency and number of landslides predicted to occur in three basins of different sizes. Ninety percent of landslides occur within a period of 20 years after a wildfire at the source. Frequency and magnitude (number of failures) of landsliding episodes grow with increasing basin size because of the larger number of landslide source areas (hollows) and the increasing probability of forest-destroying wildfires intersected by large storms.

management, or climatically induced cover change), and topography. Extensive surveys of sediment depth and the increasing availability of age data for sediment accumulations, from dendrochronology and radiocarbon measurements on charcoal and buried wood, will be needed for such tests. Short-term tests could also be carried out after major fires or storms through surveys of the conditions (especially of soil depth and topography) which caused failures or allowed the survival of colluvial wedges. The distributions of sediment depths in first- and second-order channels after fires or timber harvest could provide other opportunities. In addition, there is room for improvement and testing of individual modules of the simulation, including modules that already in use by others. These include the acceptability of the infinite-slope stability model, the role of tree-root reinforcement, and the exponential probability distributions of rainfall and fire size. We have simply worked through the consequences of these generally accepted, but weakly verified beliefs.

Even in its simplified form, the analysis illustrates how the variability of sediment supply can be analyzed in an orderly fashion as the product of particular processes and environmental controls. It indicates how certain landscape characteristics, such as typical frequency distributions of colluvium depth or of sediment loading in low-order channels, might arise and how they indicate the potential for catastrophic sedimentation. Our model provides a way of estimating, on the basis of local or transferable measurements, the approximate distribution and magnitude of sediment loading by interacting sediment transfer processes in the event of a storm, fire, or other disturbance of some anticipated scale. It indicates, for example, why most first- and second-order channels in some part of a mountain region might contain little sediment, whereas other channels in sharply bounded parts of the region might be heavily loaded, sometimes with the changes in first-order and second-order channels being out of phase.

Though based on physical principles concerning climate, fire ignition and spread, hillslope hydrology and stability, and debris-flow behavior, specific applications of the general principle of stochastic erosion and sediment supply depend heavily on empirical information, some of which is poorly constrained at present. The complexity of the data requirements, however, reflects the real complexity of spatially variable properties and process interactions in a landscape, and the articulation of these factors makes explicit some effects that are either ignored in deterministic analyses of erosion processes or are expressed only in words [e.g., *Reneau and Dietrich*, 1990].

Most of the parameters used here are already standard in analyses of landsliding (hillslope angle, hillslope or hollow length, the depth and geotechnical properties of colluvium, and the size of rainstorms); we have simply emphasized that there are consequences of the fact that these characteristics have probability distributions rather than single values. We have also emphasized that the stability of colluvium changes over millennia as it thickens and over decades after disturbance of its tree cover. These facts imply that understanding temporal and spatial patterns of landsliding over long periods at regional scale, including the effects of climate history, requires knowledge of colluvium production rates, colluvium thickening rates (and therefore landslide scar geometry), and the temporal evolution of root reinforcement. Our model also formalizes the interpretation of how the probability distributions of storms and forest-replacing fires control the magnitude of pulses of sediment from drainage areas of varying size. Finally, it illustrates the role of hollow-channel topology in modulating sediment delivery by debris flow.

With continued improvement in regional databases of rates, timing, and controls of sediment mobilization (using methods reviewed by *Reid and Dunne* [1996], for example) the approach that we have outlined could be used for analyses of such phenomena as differences in sediment delivery regimes between climatic, lithologic, or forest regions; the expected effect of climate change on sedimentation regimes (incorporating, for example, reasonable changes in the probability distributions of rainstorm and fire characteristics, and changes in root strength to match expected changes in vegetation cover); or the impact of fire suppression or radical land-use change on sedimentation regimes. The danger would lie in using the model for detailed prescriptions and small areas in the face of large uncertainties about some of the quantities to be estimated. This model is offered as a means of organizing information and analyses of the often confusing issue of sediment supply at the drainage basin scale.

In a companion paper [*Benda and Dunne*, this issue] we use the model simulations of timing, volumes, and locations of sediment influx to channels to investigate how mass wasting, fluvial sediment transport, storage in fans and terraces, and particle abrasion might influence the frequency and magnitude of sediment routing and storage in river channel networks.

**Acknowledgments.** This work was supported by Cooperative Agreements PNW 93-0422 and 94-0574 with the U.S. Forest Service Pacific Northwest Forest and Range Experiment Station, Portland. We are grateful to R. L. Bras, V. K. Gupta, and I. Rodriguez-Iturbe for stimulating our original interest in stochastic forcing of geomorphic processes at a workshop on scale effects in hydrology, to F. J. Swanson for many discussions of its application to mass wasting in the Pacific Northwest, and to J. K. Agee for advice on the application of his fire model and its extension to the form used here. Daniel Miller assisted us at many stages of the work with insightful suggestions and with computing. J. Gabrielson wrote the computer program, and H. A. Froehlich and K. Lautz provided the rainfall data for the study basin. We also appreciate improvements to the manuscript suggested by T. E. Lisle, D. R. Montgomery, C. Paola, and L. M. Reid.

## References

Agee, J. K., *Fire Ecology of Pacific Northwest Forests*, 493 pp., Island Press, Washington, D. C., 1993.

Agee, J. K., and R. Flewelling, A fire cycle model based on climate for the Olympic Mountains, Washington, in *Proceedings of Seventh Conference on Fire and Forest Meteorology*, vol. 7, pp. 32–37, Am. Meteorol. Soc., Boston, Mass., 1983.

Agee, J. K., and M. H. Huff, Fuel succession in a western hemlock/Douglas-fir forest, *Can. J. For. Res*., *17*, 697–704, 1987.

Andrews, H. J., and R. W. Cowlin, Forest resources of the Douglas-fir region. *U.S. Dep. of Agric. Misc. Publ. 389*, 169 pp., 1934.

Baldwin, E. M., Eocene stratigraphy in southwestern Oregon, *Oreg. Dep. Geol. Miner. Ind. Bull. 96*, 40 pp., 1974.

Barnosky, C. W., A record of late Quaternary vegetation from Davis Lake, southern Puget Lowland, Washington, *Quat. Res*., *16*, 221–239, 1981.

Benda, L., Debris flows in the Oregon Coast Range, M.S. thesis, 127 pp., Univ. of Wash., Seattle, 1988.

Benda, L., The influence of debris flows on channels and valley floors of the Oregon Coast Range, U.S.A., *Earth Surf. Processes Landforms*, *15*, 457–466, 1990.

Benda, L., *Stochastic geomorphology in a humid mountain landscape*, Ph.D. thesis, 353 pp., Univ. of Wash., Seattle, 1994.

Benda, L., and T. W. Cundy, Predicting deposition of debris flows in mountain channels, *Can. Geotech. J*., *27*, 409–417, 1990.

Benda, L., and T. Dunne, Sediment routing by debris flow, *Proceedings, Symposium on Erosion and Sedimentation in the Pacific Rim*, *IAHS Publ. 165*, 213–223, 1987.

Benda, L., and T. Dunne, Stochastic forcing of sediment routing and storage in channel networks, *Water Resour. Res*., this issue.

Benda, L., Miller, D. J., Dunne, T., Reeves, G. H., and Agee, J. K., Dynamic Landscape Systems, in *Ecology and Management of Streams and Rivers of the Pacific Rim*, edited by R. Naiman and R. Bilby, Springer-Verlag, New York, in press, 1997.

Beschta, R. L., River channel response to accelerated mass soil erosion, in *Proceedings of Symposium on Effects of Forest Land Use on Erosion and Slope Stability*, pp. 155–164, East–West Cent., Univ. of Hawaii, Honolulu, 1984.

Beven, K., Towards the use of catchment geomorphology in flood frequency predictions, *Earth Surf. Processes Landforms*, *12*, 69–82, 1987.

Burroughs, E. R., Landslide hazard rating for portions of the Oregon Coast Range, in *Proceedings of Symposium on Effects of Forest Land Use on Erosion and Slope Stability*, pp. 265–274, East–West Cent., Univ. of Hawaii, Honolulu, 1984.

Burroughs, E. R., and B. R. Thomas, Declining root strength in Douglas fir after felling as a factor in slope stability, *Res. Pap. INT Intermt. For. Range Exp. Stn. INT-190*, 27 pp., 1977.

Bush, G., Landslide Survey—1981–1982, Summary sheet and worksheets, Siuslaw Natl. For. Headquarters, Corvallis, Oreg., 1983.

Coates, R., and L. Collins, Streamside landsliding and channel change in a suburban forested watershed: effects of an extreme event, in *Proceedings of Symposium on Effects of Forest Land Use on Erosion and Slope Stability*, pp. 155–164, East–West Cent., Univ. of Hawaii, Honolulu, 1984.

Crozier, M. J., E. E. Vaughan, and M. J. Tippett, Relative instability of colluvium-filled bedrock depressions, *Earth Surf. Processes Landforms*, *15*, 329–339, 1990.

Cwynar, L. C., Fire and the forest history of the North Cascade Range, *Ecology*, *68*, 791–802, 1987.

Dietrich, W. E., and T. Dunne, Sediment budget for a small catchment in mountainous terrain, *Z. Geomorph. Suppl*., *29*, 191–206, 1978.

Dietrich, W. E., T. Dunne, N. F. Humphrey, and L. M. Reid, Construction of sediment budgets for drainage basins, in *Sediment Budgets and Routing in Forested Drainage Basins*, *Gen. Tech. Rep. PNW Pac. Northwest For. Range Exp. Stn. PNW-141*, 5–23, 1982.

Dietrich, W. E., C. J. Wilson, and S. L. Reneau, Hollows, colluvium, and landslides in soil-mantled landscapes, in *Hillslope Processes*, edited by A. D. Abrahams, pp. 361–388, Allen and Unwin, Winchester, Mass., 1986.

Dunne, T., Stochastic aspects of the relations between climate, hydrology and landform evolution, *Trans. Jpn. Geomorphol. Union*, *12*, 1–24, 1991.

Eagleson, P. S., Dynamics of flood frequency, *Water Resour. Res*., *8*, 878–898, 1972.

Franklin, J. F., and C. T. Dyrness, Natural vegetation of Oregon and Washington, *Gen. Tech. Rep. PNW Pac. Northwest For. Range Exp. Stn. PNW-8*, 417 pp., 1973.

Gresswell, S., D. Heller, and D. N. Swanston, Mass movement response to forest management in the central Oregon Coast Range, *Resour. Bull. PNW Pac. Northwest For. Range Exp. Stn. PNW-84*, 1979.

Griffiths, G. A., Recent sedimentation history of the Waimakariri River, New Zealand, *J. Hydrol. N. Z*., *18*, 6–28, 1979.

Hack, J. T., and J. C. Goodlett, Geomorphology and forest ecology of a mountain region in the Central Appalachians, *U.S. Geol. Surv. Prof. Pap. 347*, 66 pp., 1960.

Hammond, C., D. Hall, S. Miller, and P. Swetik, Level 1 stability analysis (LISA), documentation of version 2.0, *U.S. For. Ser. Gen. Tech. Rep. INT-285*, 190 pp., 1992.

Harr, R. D., Water flux in soil and subsoil on a steep forested slope, *J. Hydrol.*, *33*, 37–58, 1977.

Heusser, C. J., Quaternary vegetation, climate and glaciation in the Hoh River valley, Washington, *Geol. Soc. Am. Bull.*, *85*, 1547–1560, 1974.

Heusser, C. J., Quaternary palynology of the Pacific slope of Washington, *Quat. Res.*, *8*, 282–306, 1977.

Hough, B. K., *Basic Soils Engineering*, 513 pp., Ronald Press, New York, 1957.

Humphrey, N. F., Pore pressures in debris failure initiation, *Rep. A-108-WASH*, Off. of Water Resour. Technol., Seattle, Wash., 1983.

Iida, T., A hydrological method of estimation of the topographic effect on the saturated throughflow, *Trans. Jpn. Geomorphol. Union*, *5*, 1–12, 1984.

Isaac, L. A., and G. S. Meagher, Natural reproduction on the Tillamook burn four years after the fire, *Rep. Pac. Northwest For. Exp. Stn.*, 1936.

Johnson, D. L., The late Quaternary climate of coastal California: Evidence for an ice age refugium, *Quat. Res.*, *8*, 154–179, 1976.

Ketcheson, G., and H. A. Froehlich, Hydrologic factors and environmental impacts of mass soil movements in the OCR, 94 pp., Water Resour. Res. Inst., Oreg. State Univ., Corvallis, 1978.

Lehre, A. K., Sediment budget of a small Coast Range Drainage Basin in North-Central California, in *Sediment Budgets and Routing in Forested Drainage Basins*, *Gen. Tech. Rep. PNW Pac. Northwest For. Range Exp. Stn. PNW-141*, 67–77, 1982.

Leopold, E. B., R. Nickmann, J. I. Hedges, and J. R. Ertel, Pollen and lignin records of the late Quaternary vegetation, Lake Washington, *Science*, *218*, 1305–1307, 1982.

Lisle, T. E., Effects of aggradation and degradation on pool-riffle morphology in natural gravel channels, northwestern California, *Water Resour. Res.*, *18*, 1643–1651, 1982.

Long, C. J., Fire history of the Central Oregon Coast Range, Oregon: 9000-year record from Little Lake, M.S. thesis, 147 pp., Univ. of Oreg., Eugene, 1995.

Madej, M. A., and V. Ozaki, Channel response to sediment wave propagation and movement, Redwood Creek, California, USA, *Earth Surf. Processes Landforms*, *21*, 911–927, 1996.

Montgomery, D. R., Channel Initiation and landscape evolution, Ph.D. thesis, 421 pp., Univ. of Calif., Berkeley, 1991.

Nakamura, F., Chronological study on the torrential channel bed by the age distribution of deposits, *Res. Bull. Coll. Exp. For. Hokkaido Univ.*, *43*, 1–26, 1986.

O'Connor, M. D., Sediment transport in steep tributary streams and the influence of large organic debris, Ph.D. thesis, 317 pp., Univ. of Wash., Seattle, 1994.

Ohmori, H., and M. Hirano, Magnitude, frequency and geomorphological significance of rocky mud flows, land creep and the collapse of steep slopes, *Z. Geomorph. Suppl.*, *67*, 55–65, 1988.

Okunishi, K., and T. Iida, Evolution of hillslopes including landslides, *Trans. Jpn. Geomorphol. Union*, *2*, 291–300, 1981.

O'Loughlin, C., and A. J. Watson, Root-wood strength deterioration in *Radiata* Pine after clearfelling, *N. Z. J. For. Sci.*, *9*, 284–293, 1979.

Ouchi, S., Tombi landslide and its impact on the Joganji River, Japan, in *Proceedings, Symposium on Erosion and Sedimentation in the Pacific Rim*, *IAHS Publ. 165*, 135–136, 1987.

Pearce, A. J., and A. J. Watson, Effects of earthquake-induced landslides on sediment budget and transport over a 50-yr period, *Geology*, *14*, 52–55, 1986.

Perkins, S. J., Landslide deposits in low-order streams—their erosion rates and effects on channel morphology, in *Proceedings, Symposium on Headwater Hydrology*, *TPS-89-1*, pp. 173–182, Am. Water Resour. Assoc., Bethesda, Md., 1989.

Personius, S. F., H. M. Kelsey, and P. C. Grabau, Evidence for regional stream aggradation in the central Oregon Coast Range during the Pleistocene-Holocene transition, *Quat. Res.*, *40*, 297–308, 1993.

Pickup, G., R. J. Higgins, and I. Grant, Modelling sediment transport as a moving wave—the transfer and deposition of mining waste, *J. Hydrol.*, *60*, 281–301, 1983.

Pierson, T. C., Factors controlling debris-flow initiation on forested hillslopes in the Oregon Coast Range, Ph.D. dissertation, 167 pp., Univ. of Wash., Seattle, 1977.

Reid, L. M., and T. Dunne, *Rapid Construction of Sediment Budgets for Drainage Basins*, 160 pp., Catena-Verlag, Cremlingen, Germany, 1996.

Reneau, S. L., Depositional and erosional history of hollows: Application to landslide location and frequency, long-term erosion rates and the effects of climate change, Ph.D. thesis, 328 pp., Univ. of Calif., Berkeley, 1988.

Reneau, S. L., and W. E. Dietrich, Depositional history of hollows on steep slopes, coastal Oregon and Washington, *Nat. Geogr. Res.*, *6*, 220–230, 1990.

Reneau, S. L., and W. E. Dietrich, Erosion rates in the southern Oregon Coast Range: Evidence for an equilibrium between hillslope erosion and sediment yield, *Earth Surf. Processes Landforms*, *16*, 307–322, 1991.

Roberts, R. G., and M. Church, The sediment budget in severely disturbed watersheds, Quee Charlotte Ranges, British Columbia, *Can. J. For. Res.*, *16*, 1092–1106, 1986.

Roth, G., F. Siccardi, and R. Rosso, Hydrodynamic description of the erosional development of drainage patterns, *Water Resour. Res.*, *25*, 319–332, 1989.

Schroeder, W. L., and J. V. Alto, Soil properties for slope stability analysis: Oregon and Washington Coastal Mountains, *For. Sci.*, *29*, 823–833, 1983.

Sidle, R. C., A dynamic model of slope stability in zero-order basins, *Proceedings, Symposium on Erosion and Sedimentation in the Pacific Rim*, *IAHS Publ. 165*, 101–110, 1987.

Sidle, R. C., A conceptual model of changes in root cohesion in response to vegetation management, *J. Environ. Qual.*, *20*, 43–52, 1991.

Sidle, R. C., A theoretical model of the effects of timber harvesting on slope stability, *Water Resour. Res.*, *28*, 1897–1910, 1992.

Swanson, F. J., Fire and geomorphic processes, in *Fire Regimes and Ecosystem Properties*, *Gen. Tech. Rep. WO U.S. For. Serv. WO-26*, 401–420, 1981.

Swanson, F. J., and G. W. Lienkaemper, Physical consequences of large organic debris in Pacific Northwest streams, *Gen. Tech. Rep. PNW Pac. Northwest For. Range Exp. Stn. PNW-69*, 12 pp., 1978.

Swanson, F. J., M. M. Swanson, and C. Woods, Analysis of debris avalanche erosion in steep forested lands: An example from Mapleton, Oregon, U.S., in *Proceedings, Symposium on Erosion and Sediment Transport in the Pacific Rim Steeplands*, *IAHS Publ. 132*, 67–75, 1981.

Swanson, F. J., R. L. Fredriksen, and F. M. McCorison, Material transfer in a western Oregon forested watershed, in *Analysis of Coniferous Forest Ecosystems in the Western United States*, edited by R. L. Edmonds, pp. 233–266, Hutchinson Ross, Stroudsburg, Pa., 1982.

Teensma, P. D. A., Fire history and fire regimes of the central western Cascades of Oregon. Ph.D. thesis, 188 pp., Univ. of Oreg., Eugene, 1987.

Teensma, P. D. A., J. T. Rienstra, and M. A. Yeiter, Preliminary reconstruction and analysis of change in forest stand age classes of the OCR from 1850 to 1940, *Tech. Note T/N OR-9*, 7 pp., Bur. of Land Manage., Washington, D. C., 1991.

Tsukamoto, Y., and H. Minematsu, Hydrogeomorphological characteristics of a zero-order basin, in *Proceedings, Symposium on Erosion and Sedimentation in the Pacific Rim*, *IAHS Publ. 165*, 61–70, 1987.

U.S. Weather Bureau, Generalized estimates of probable maximum precipitation for the United States west of the 105th meridian for areas to 400 square miles and duration to 24 hours, *Tech. Pap. 38*, 66 pp., 1960.

Van Wagner, C. E., Age-class distribution and the forest fire cycle, *Can. J. For. Res.*, *8*, 220–227, 1978.

Wilson, C. J., and W. E. Dietrich, The contribution of bedrock groundwater flow to storm runoff and high pore pressure development in hollows, in *Proceedings, Symposium on Erosion and Sedimentation in the Pacific Rim*, *IAHS Publ. 165*, 49–60, 1987.

Worona, M. A., and C. Whitlock, Late Quaternary vegetation and climate history near Little Lake, central Coast Range, Oregon, *Geol. Soc. Am. Bull.*, *107*, 867–876, 1995.

Ziemer, R. R., Roots and the stability of steep slopes, in *Proceedings, Symposium on Erosion and Sediment Transport in Pacific Rim Steeplands*, *IAHS Publ. 132*, 343–357, 1981.

L. Benda, Earth Systems Institute, 1314 NE 43rd St., Suite 207, Seattle, WA 98105-5832. (email: leebenda@aol.com)

T. Dunne, School of Environmental Science and Management, University of California, 4670 Physical Sciences North, Santa Barbara, CA 93106-5131. (email: tdunne@esm.ucsb.edu).

(Received October 23, 1995; revised August 18, 1997;
accepted August 22, 1997.)